Fig. 2. Cytotoxicity of HPMA-ZnPP with light-irradiation via singlet oxygen generation. (A) ESR spectra for HPMA-ZnPP (upper panel) and ZnPP (lower panel) dissolved in PBS or in PBS containing 0.5% Tween 20 plus light irradiation for the indicated times. $^1O_2$ generated here was captured by 4-oxo-TEMP, and triplet 4-oxo-TEMPO signal due to $^1O_2$ was detected by ESR spectra. HPMA-ZnPP with Tween 20 plus light exposure considerably enhanced $^1O_2$ generation in an exposure-time-dependent manner. (B) HeLa cells, plated in 96-well plates, were treated with increasing concentrations of ZnPP or HPMA-ZnPP for 72 h. At 24 h after treatment, cells were irradiated with light and were incubated for another 48 h. The MTT assay was used to quantify surviving cells, as a ratio of the surviving fraction to the untreated control. Values (%) are means surviving cells ± s.d. (C) Effect of medium change and light induced toxicity against HeLa cells in culture. Here fresh medium was replaced for spent medium to remove free ZnPP or HPMA-ZnPP and light was irradiated. Cell survival was quantified as in Fig. 2A. (D) Disintegration of HPMA-ZnPP micelles at 10 μg/ml as determined by fluorescence spectra in the presence of increasing concentrations of egg lecithin at 25 °C for 30 min. (E) Disintegration of HPMA-ZnPP at 10 μg/ml as determined by increasing concentrations (60–600 μg/ml) of lecithin and fluorescence intensity at 25 °C for indicated times.

exhibit light-induced cytotoxicity, HPMA-ZnPP micelles must be disintegrated after cellular internalization. We thus examined the effect of cellular components; cell membrane and constituents of the lipid bilayer such as lecithin. Interestingly addition of lecithin disintegrated HPMA-ZnPP micelles as seen by the increase of fluorescence intensity (Fig. 2D). We recently reported that SMA-ZnPP underwent disintegration in cells, which was caused by the cell membrane and its component lecithin [25]. We found that fluorescence intensity of HPMA-ZnPP micelles clearly increased after addition of lecithin in a dose- and time-dependent manner (Fig. 2D, E). The same was seen after addition of cell membrane fractions of tumor and liver (data not shown).

3.7. Antitumor activity of HPMA-ZnPP in vivo

The antitumor effect of HPMA-ZnPP micelles was examined with S-180 tumor in mice. After 24, 48 and 72 h i.v. injection of HPMA-ZnPP micelles, tumors on the dorsal skin were irradiated with xenon light (20 mW/cm²; 400–800 nm) for 5 min. Tumor sizes of two control

groups which one without drug, and the other treated with HPMA-ZnPP micelles but without light irradiation increased; however, the tumor size in the group administered with the drug plus light-irradiation was reduced significantly (Fig. 3).

3.8. Cell uptake of HPMA-ZnPP

Consistent with our previous report [25], tumor cells internalized free ZnPP efficiently; however, far less HPMA-ZnPP was internalized, only about 2.5% of free ZnPP, at least up to 6 h of incubation (Fig. 4A). HPMA-ZnPP internalization was also suppressed at a low temperature (4 °C), which suggests that HPMA-ZnPP was internalized via the endocytic pathway (Fig. 4B).

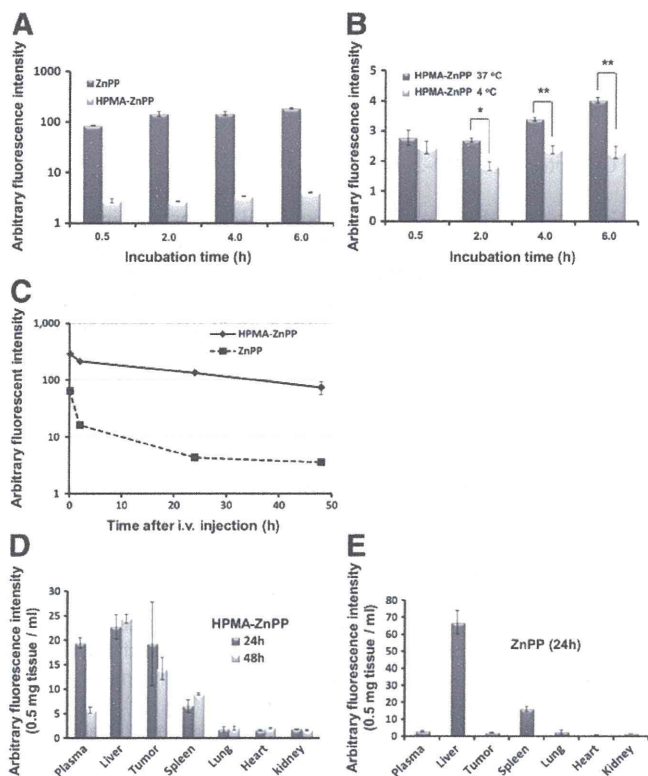### 3.9. Pharmacokinetics, organ distribution of HPMA-ZnPP after i.v. administration

We quantified the concentration of free ZnPP and HPMA-ZnPP micelles in the blood after i.v. injection. Free ZnPP was rapidly cleared from the systemic circulation; however, HPMA-ZnPP micelles remained in the circulation for much prolonged time, i.e. $t_{1/2}$ in plasma was about 24 h (Fig. 4C). Examination of the organ distribution of HPMA-ZnPP micelles 24 and 48 h after i.v. injection demonstrated marked accumulation of HPMA-ZnPP micelles in the tumor as well as in the liver at 24 and 48 h (Fig. 4D). In contrast, free ZnPP was found mostly in the liver, and less in the spleen, and not in the tumor (Fig. 4E). The amount of HPMA-ZnPP micelles accumulated in tumor was about 10 times more than that in the lung, kidney and heart (Fig. 4D).

3.10. In vivo fluorescence imaging after i.v. injection of HPMA-ZnPP

Fluorescence imaging using the in vivo fluorescence imaging system (IVIS Lumina-XR) confirmed the selective accumulation of HPMA-ZnPP micelles in tumor. At 24 h after i.v. injection of HPMA-ZnPP micelles, preferential fluorescence of tumor tissue was observed by excitation at 430 ± 15 nm (Fig. 5A, cf. 5A′). Furthermore, when we examined each dissected tissue, only tumor tissue fluoresced, while little appreciable fluorescence of normal tissues including the kidney, liver, lung and skin (Fig. 5B, cf. 5B′). Regardless of the accumulation of HPMA-ZnPP and free ZnPP in the liver, showed in Fig. 4D and E, fluorescence at the liver was unremarkable. This discrepancy of least fluorescence of the liver may be attributed to the high content of heme protein in the liver, which might disturb the transmission of excitation light and/or absorb the fluorescence emission, thus least fluorescence was detected in the liver. These data suggest that HPMA-ZnPP micelles can selectively accumulate in tumor tissue and it can be used for sensitive visualization
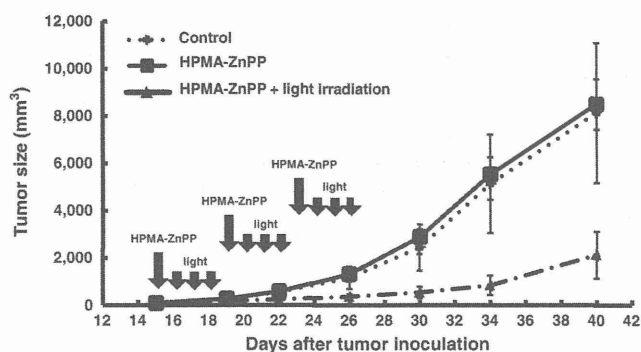
Fig. 3. Light-irradiation induced antitumor activity of HPMA-ZnPP. HPMA-ZnPP was administered at 15 mg of ZnPP per kg equivalent followed by xenon light-irradiation at the indicated times. S-180 tumor volume (mm3) was calculated as (W²×L)/2, where L = longitudinal and W = width of the tumor.

Fig. 4. Intracellular uptake, in vivo pharmacokinetics and body distribution of HPMA-ZnPP micelle. (A) Cell uptake of HPMA-ZnPP and free ZnPP by HeLa cells. ZnPP or HPMA-ZnPP (20 μg/ml ZnPP equivalent dose) was administered for the indicated time periods. After cells were washed, intracellular ZnPP or HPMA-ZnPP was extracted in ethanol, and quantified by fluorescence intensity of ZnPP and HPMA-ZnPP was measured by fluorescence spectroscopy. (B) Effect of temperature for cell uptake of HPMA-ZnPP. The methods used as same as in (A) above. Values are means ± s.d. **P<0.01 and *P<0.05, significant differences, according to Student's t-test. (C) Blood profile of free ZnPP or HPMA-ZnPP at 18 mg of ZnPP equivalent per kg was injected i.v. into S-180 tumor-bearing mice. ZnPP concentration was determined by fluorescence intensity. (D) (E) Tissue distribution of HPMA-ZnPP and free ZnPP at 24 and 48 h after injection of 15 mg of ZnPP equivalent/kg of (D) HPMA-ZnPP, or (E) free ZnPP. Mice were sacrificed and HPMA-ZnPP or ZnPP in each tissue was extracted with DMSO and quantified as in (C).

of tumor with use of the appropriate spectroscopic system, which simultaneously exerting therapeutic effects via generation of $^1O_2$.

4. Discussion

We report here chemical conjugation of ZnPP with a highly biocompatible HPMA copolymer to produce HPMA-ZnPP (Scheme 1). As Scheme 1 illustrates, the carboxyl group of free ZnPP was conjugated to the hydroxyl group and the terminal amino group of HPMA. This pendant-type conjugation improved ZnPP loading about 3–4 fold of PEG-ZnPP, another ZnPP polymer conjugate prepared in our laboratory previously, via ester and amide bonds when we compared with one ZnPP at the terminal end of PEG [21]. We thus achieved 20% loading of ZnPP with good water solubility, more than 30 mg/ml HPMA-ZnPP in distilled water.

HPMA-ZnPP consisted of hydrophilic chain of HPMA and hydrophobic chromophore, ZnPP. This amphiphilic characteristic would be expected to result in spontaneous micelles formation in aqueous solution. The apparent hydrodynamic diameter of HPMA-ZnPP micelles in aqueous solution exhibited a single peak distribution having mean particle diameter of 82.8 ± 41.8 nm as determined by dynamic light scattering (Fig. 1D-i, -ii), and Sephacryl S-300 chromatography

showed a single peak of apparent MW of HPMA-ZnPP were 198-kDa (data not shown). Furthermore, transmission electron microscopy revealed that HPMA-ZnPP forms round micelles (Fig. 1E).

HPMA polymer at a MW about 12-kDa was estimated to have a linear size of approximately 15 nm, and its hydrodynamic diameter in PBS was about 5.6 ± 1.9 nm as determined by dynamic light scattering in PBS (pH 7.4). These data suggest that several HPMA-ZnPP conjugates cluster together to form HPMA-ZnPP micelles with a mean particle diameter of 82.8 nm. It is considered that interactions of hydrophobic ZnPP residues as head group would together form this micellar structure, in which hydrophilic HPMA tail chain would form a hydrophilic outer surface layer facing water in the milieu.

Fig. 1C showed that the covalent bond (perhaps ester linkage) between ZnPP and HPMA was efficiently cleaved when HPMA-ZnPP micelle was disrupted in the organic solvent (DMSO) and exposed to an alkaline solution (10 mM NaOH). This result suggests that the ZnPP part of the HPMA-ZnPP micelle is embedded in a hydrophobic core, so access of OH− is very little and as a result cleavage was slow in aqueous solutions as far as HPMA-ZnPP remains in micellar form. Fig. 1F, G and H showed that HPMA-ZnPP micelles were dissociated by detergents such as Tween 20, and sodium dodecyl sulfate (data not shown) but not by urea, which suggests that ZnPP is clustered in aqueous solution by hydrophobic interaction, not by hydrogen bonding. In contrast to the present finding, SMA complexed with ZnPP was dissociated by either detergents or 9 M urea (our unpublished data). It is noteworthy that fluorescence due to ZnPP is almost completely quenched (Figs. 1G, H, 2D) and micelle disruption regenerates fluorescence. Dissociation of HPMA-ZnPP micelles by cell-membrane components or lecithin also led to regeneration of fluorescence as indication of micellar disruption in the cells. Furthermore, generation of $^1O_2$ by light irradiation can be achieved more effectively when the micelles were disintegrated (Fig. 2A). This mean when micelles are in circulation they do not emit fluorescence nor $^1O_2$.

The molecular target of ZnPP, ie, HO-1 is located in the endoplasmic reticulum in the cells, thus ZnPP micelles must be internalized by cells in order to exert HO-1 inhibition which leads to cell death due to increased oxystress [25–28]. We recently showed that SMA-ZnPP was efficiently internalized by cells and exhibited cytotoxicity comparable to that of native free ZnPP; in contrast PEG-ZnPP showed much slower intracellular uptake thereby showed little cytotoxicity [25]. We found that intracellular uptake of HPMA-ZnPP was much slower than that of free ZnPP (Fig. 4A) and that HPMA-ZnPP by itself showed little cytotoxic activity against HeLa cells in vitro; even at 100 μg/ml ZnPP equivalent, unless light irradiation was applied (Fig. 2B). This low cytotoxic effect may be explained by low HO-1 inhibitory activity in the cells. HPMA-ZnPP micelles exhibited less than 10% of HO-1 inhibitory activity compared to ZnPP in a cell-free system (data not shown). The reason for this low activity may be that ZnPP is not available to interact with HO-1 because ZnPP may be stacked together in the inner core of the HPMA-ZnPP micelles. This hypothesis agrees well with our observation illustrated in Fig. 1C; DMSO disintegrated the micellar form of HPMA-ZnPP, and thus micelles become single HPMA-ZnPP chain and its ester bonding may be hydrolyzed by alkaline (OH−). Thus, HPMA-ZnPP micelles alone were not expected to exhibit anticancer activity. Consistent with this interpretation and expectation, HPMA-ZnPP alone showed no antitumor activity in vivo against S-180 tumor in mice (Fig. 3).

In contrast to above observation, however, light-irradiation greatly enhanced the cytotoxic effect of HPMA-ZnPP micelles in in vitro and in vivo (Figs. 2B and 3). In HPMA-ZnPP micelles, ZnPP probably forms a π–π stacked structure, and excited fluorochrome dissipates the energy, so neither fluorescence nor $^1O_2$ formation occurs. However, when micelles are disintegrated by detergents such as Tween 20, HPMA-ZnPP can generate $^1O_2$ under light irradiation (Fig. 2A). Consequently, we found that HPMA-ZnPP exerted cytotoxicity with light-irradiation. These results indicate that HPMA-ZnPP micelles may exist as a
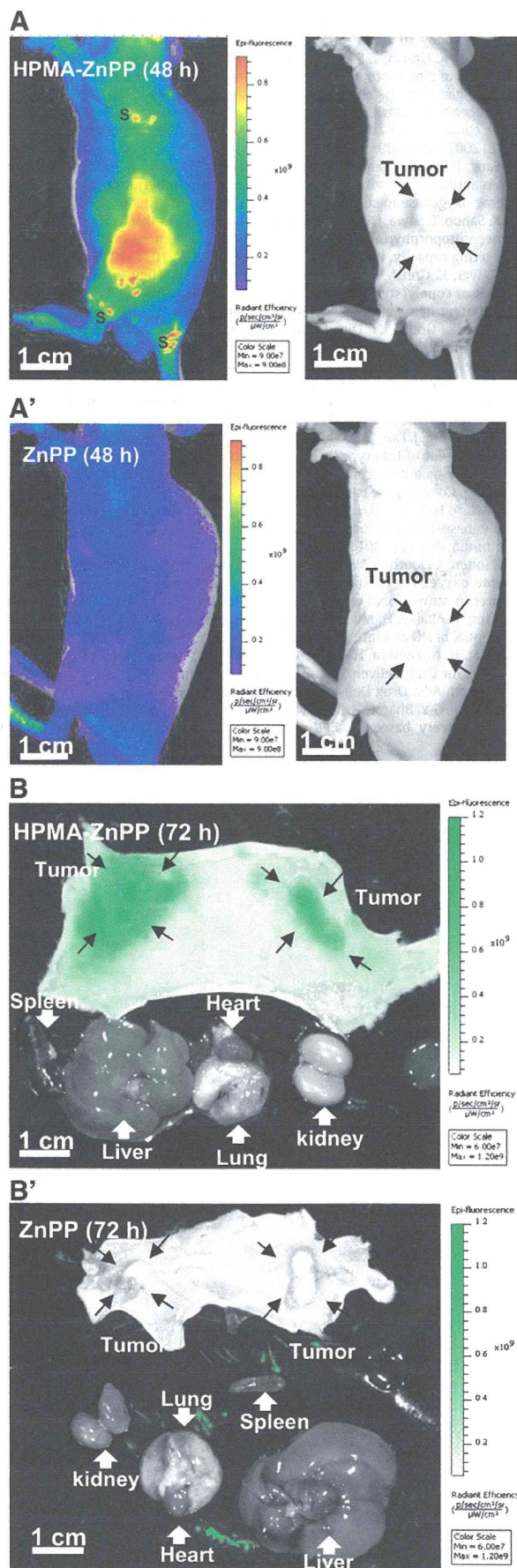
disintegrated form in the cells after intracellular internalization. We recently found that SMA-ZnPP undergoes disintegration in cells, which is caused by the cell membrane component lecithin as described [25]. We therefore anticipated that HPMA-ZnPP would be also disintegrated, as we demonstrated by adding lecithin (Fig. 2D, E).

The first critical step in selective delivery of anticancer drugs to tumors is to utilize the EPR effect. Biocompatible macromolecules of more than 40 kDa (size above 10 nm) with a neutral to slightly anionic charge are expected to accumulate in tumors via the EPR effect [9–11,29,30]. As described above, HPMA-ZnPP micelles exhibited a mean hydrodynamic diameter of about 80 nm with a zeta potential of + 1.12 mV. These data indicate that HPMA-ZnPP micelles would be preferentially accumulated in tumors by EPR effect-driven mechanism.

We found that the blood half-life of HPMA-ZnPP micelles was markedly longer (> 40 times) than that of free ZnPP and thus HPMA-ZnPP micelles accumulated about 10 times more in tumor than in lung, kidney and heart (Fig. 4D, E). This tumor accumulation property of HPMA-ZnPP is superior to our previous report on ZnPP micelles, i.e. SMA-ZnPP and PEG-ZnPP, having tumor/normal tissue (lung, kidney and heart) ratio of approx. 0.8–1 and 2–3 respectively [20,23]. Because of a slower intracellular uptake and lower HO-1 inhibition, HPMA-ZnPP alone showed no appreciable antitumor activity even with excessive tumor accumulation of HPMA-ZnPP (approximately 5–10 times greater than the lung or kidney, i.e. 200–300 µg/g of tissue).

Of greater interest in conjunction with fluorescence endoscopy, we found that HPMA-ZnPP micelles may be useful as a fluorescence tumor imaging probe. It emits fluorescence and produce $^1O_2$ upon light irradiation (Figs. 1G and 2A). Thus, HPMA-ZnPP micelles can be used as fluorescent nanoprobes in fluorescence endoscopy also for probe for PDT.

A xenon light source, which is usually used in conventional endoscopy, can be readily utilized in this fluorescent method. Xenon light used in the endoscope emits light with a wide spectral wavelength range, from 400 to 750 nm, so any fluorescent probe can be adapted as described here. Near-infrared light has been thought to be more useful because of better tissue penetration, although heat that is generated causes serious inconvenience. The present results in mice, however, demonstrated tumors implanted in mice readily detectable, and indicate that superficial tumors such as ductal tumors as esophageal or colonic tumor can be detected similarly. We believe therefore that the ductal tumors such as esophageal, gastric or cavity tumors of colon, uterine and urinary bladder or even abdominal and pleural cavity are ideal for application of this fluorescence endoscopy. Furthermore, the present results suggest an effective PDT by using conventional endoscopy equipped with xenon lamp would warrant noninvasive highly sensitive theranostic modality for solid tumor. Studies along this line are under way in our laboratory.

Acknowledgments

Fig. 5. In vivo fluorescence imaging of tumors using HPMA-ZnPP. (A) (A′) Whole-body fluorescent views of tumor-bearing mice after injection with HPMA-ZnPP (A) and free ZnPP (A′), respectively. Images were obtained 48 h after i.v. drug injection (both at 15 mg/kg ZnPP equivalent). (B) (B′) Dissected tissues of mice corresponding to (A) and (A′) under fluorescent light, with images obtained at 72 h after i.v. injection. Only tumor nodules in (A) and (B) are fluorescent.

References

[1] K. Berg, P.K. Selbo, A. Weyergang, A. Dietze, L. Prasmickaite, A. Bonsted, B.O. Engesaeter, E. Angell-Petersen, T. Warloe, N. Frandsen, A. Hogset, Porphyrin-related photosensitizers for cancer imaging and therapeutic applications, J. Microsc. 218 (Pt 2) (2005) 133–147.

[2] S.K. Pushpan, S. Venkatraman, V.G. Anand, J. Sankar, D. Parmeswaran, S. Ganesan, T.K. Chandrashekar, Porphyrins in photodynamic therapy — a search for ideal photosensitizers, Curr. Med. Chem. Anticancer Agents 2 (2) (2002) 187–207.

[3] I. Rodica-Mariana, Synthetic metallo-porphyrins and selection criteria for PDT, Oftalmologia 56 (1) (2003) 83–88.

[4] S. Tsukagoshi, Development of a novel photosensitizer, talaporfin sodium, for the photodynamic therapy (PDT), Gan To Kagaku Ryoho 31 (6) (2004) 979–985.

[5] J. Usuda, H. Kato, T. Okunaka, K. Furukawa, H. Tsutsui, K. Yamada, Y. Suga, H. Honda, Y. Nagatsuka, T. Ohira, M. Tsuboi, T. Hirano, Photodynamic therapy (PDT) for lung cancers, J. Thorac. Oncol. 1 (5) (2006) 489–493.

[6] Y. Matsumura, H. Maeda, A new concept for macromolecular therapeutics in cancer chemotherapy: mechanism of tumoritropic accumulation of proteins and the antitumor agent smancs, Cancer Res. 46 (12 Pt 1) (1986) 6387–6392.

[7] H. Maeda, Macromolecular therapeutics in cancer treatment: the EPR effect and beyond, J. Control. Release 164 (2) (2012) 138–144.

[8] H. Maeda, Y. Matsumura, EPR effect based drug design and clinical outlook for enhanced cancer chemotherapy, Adv. Drug Deliv. Rev. 63 (3) (2011) 129–130.

[9] H. Maeda, Tumor-selective delivery of macromolecular drugs via the EPR effect: background and future prospects, Bioconjug. Chem. 21 (5) (2010) 797–802.

[10] H. Maeda, Vascular permeability in cancer and infection as related to macromolecular drug delivery, with emphasis on the EPR effect for tumor-selective drug targeting, Proc. Jpn. Acad. Ser. B Phys. Biol. Sci. 88 (3) (2012) 53–71.

[11] H. Maeda, in: Polymer Conjugated Macromolecular Drugs for Tumor-specific Targeting, John Wiley & Sons Ltd, New York, 1994, pp. 353–382.

[12] Y. Noguchi, J. Wu, R. Duncan, J. Strohalm, K. Ulbrich, T. Akaike, H. Maeda, Early phase tumor accumulation of macromolecules: a great difference in clearance rate between tumor and normal tissues, Jpn. J. Cancer Res. 89 (3) (1998) 307–314.

[13] L.W. Seymour, Y. Miyamoto, H. Maeda, M. Brereton, J. Strohalm, K. Ulbrich, R. Duncan, Influence of molecular weight on passive tumour accumulation of a soluble macromolecular drug carrier, Eur. J. Cancer 31A (5) (1995) 766–770.

[14] C. He, Y. Hu, L. Yin, C. Tang, C. Yin, Effects of particle size and surface charge on cellular uptake and biodistribution of polymeric nanoparticles, Biomaterials 31 (13) (2010) 3657–3666.

[15] T. Etrych, P. Chytil, T. Mrkvan, M. Sirova, B. Rihova, K. Ulbrich, Conjugates of doxorubicin with graft HPMA copolymers for passive tumor targeting, J. Control. Release 132 (3) (2008) 184–192.

[16] K. Ulbrich, T. Etrych, P. Chytil, M. Jelinkova, B. Rihova, HPMA copolymers with pH-controlled release of doxorubicin: in vitro cytotoxicity and in vivo antitumor activity, J. Control. Release 87 (1–3) (2003) 33–47.

[17] F.M. Veronese, G. Pasut, PEGylation, successful approach to drug delivery, Drug Discov. Today 10 (21) (2005) 1451–1458.

[18] A.K. Iyer, K. Greish, T. Seki, S. Okazaki, J. Fang, K. Takeshita, H. Maeda, Polymeric micelles of zinc protoporphyrin for tumor targeted delivery based on EPR effect and singlet oxygen generation, J. Drug Target. 15 (7–8) (2007) 496–506.

[19] M. Regehly, K. Greish, F. Rancan, H. Maeda, F. Bohm, B. Roder, Water-soluble polymer conjugates of ZnPP for photodynamic tumor therapy, Bioconjug. Chem. 18 (2) (2007) 494–499.

[20] J. Fang, T. Sawa, T. Akaike, T. Akuta, S.K. Sahoo, G. Khaled, A. Hamada, H. Maeda, In vivo antitumor activity of pegylated zinc protoporphyrin: targeted inhibition of heme oxygenase in solid tumor, Cancer Res. 63 (13) (2003) 3567–3574.

[21] S.K. Sahoo, T. Sawa, J. Fang, S. Tanaka, Y. Miyamoto, T. Akaike, H. Maeda, Pegylated zinc protoporphyrin: a water-soluble heme oxygenase inhibitor with tumor-targeting capacity, Bioconjug. Chem. 13 (5) (2002) 1031–1038.

[22] A.K. Iyer, K. Greish, J. Fang, R. Murakami, H. Maeda, High-loading nanosized micelles of copoly(styrene-maleic acid)-zinc protoporphyrin for targeted delivery of a potent heme oxygenase inhibitor, Biomaterials 28 (10) (2007) 1871–1881.

[23] J. Fang, K. Greish, H. Qin, L. Liao, H. Nakamura, M. Takeya, H. Maeda, HSP32 (HO-1) inhibitor, copoly(styrene-maleic acid)-zinc protoporphyrin IX, a water-soluble micelle as anticancer agent: in vitro and in vivo anticancer effect, Eur. J. Pharm. Biopharm. 81 (3) (2012) 540–547.

[24] H. Maeda, Assay of proteolytic enzymes by the fluorescence polarization technique, Anal. Biochem. 92 (1) (1979) 222–227.

[25] H. Nakamura, J. Fang, B. Gahininath, K. Tsukigawa, H. Maeda, Intracellular uptake and behavior of two types zinc protoporphyrin (ZnPP) micelles, SMA-ZnPP and PEG-ZnPP as anticancer agents; unique intracellular disintegration of SMA micelles, J. Control. Release 155 (3) (2011) 367–375.

[26] H.P. Kim, H.O. Pae, S.H. Back, S.W. Chung, J.M. Woo, Y. Son, H.T. Chung, Heme oxygenase-1 comes back to endoplasmic reticulum, Biochem. Biophys. Res. Commun. 404 (1) (2011) 1–5.

[27] T. Linden, J. Doutheil, W. Paschen, Role of calcium in the activation of erp72 and heme oxygenase-1 expression on depletion of endoplasmic reticulum calcium stores in rat neuronal cell culture, Neurosci. Lett. 247 (2–3) (1998) 103–106.

[28] J. Fang, T. Akaike, H. Maeda, Antiapoptotic role of heme oxygenase (HO) and the potential of HO as a target in anticancer treatment, Apoptosis 9 (1) (2004) 27–35.

[29] J. Fang, H. Nakamura, H. Maeda, The EPR effect: unique features of tumor blood vessels for drug delivery, factors involved, and limitations and augmentation of the effect, Adv. Drug Deliv. Rev. 63 (3) (2010) 136–151.

[30] H. Maeda, G.Y. Bharate, J. Daruwalla, Polymeric drugs for efficient tumor-targeted drug delivery based on EPR-effect, Eur. J. Pharm. Biopharm. 71 (3) (2009) 409–419.

Advanced Drug Delivery Reviews
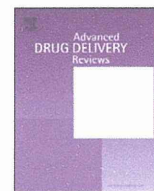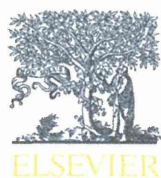
The EPR effect for macromolecular drug delivery to solid tumors: Improvement of tumor uptake, lowering of systemic toxicity, and distinct tumor imaging in vivo ☆

Hiroshi Maeda *, Hideaki Nakamura, Jun Fang

DDS Research Institute, Sojo University, 4-22-1, Ikeda, Kumamoto, 860-0082, Japan

ARTICLE INFO

ABSTRACT

The EPR effect results from the extravasation of macromolecules or nanoparticles through tumor blood vessels. We here provide a historical review of the EPR effect, including its features, vascular mediators found in both cancer and inflamed tissue. In addition, architectural and physiological differences of tumor blood vessels vs that of normal tissue are commented. Furthermore, methods of augmentation of the EPR effect are described, that result in better tumor delivery and improved therapeutic effect, where nitroglycerin, angiotensin I-converting enzyme (ACE) inhibitor, or angiotensin II-induced hypertension are employed. Consequently, better therapeutic effect and reduced systemic toxicity are generally observed. Obviously, the EPR effect based delivery of nanoprobes are also useful for tumor-selective imaging agents with using fluorescent or radio nuclei in nanoprobes. We also commented a key difference between passive tumor targeting and the EPR effect in tumors, particularly as related to drug retention in tumors: passive targeting of low-molecular-weight X-ray contrast agents involves a retention period of less than a few minutes, whereas the EPR effect of nanoparticles involves a prolonged retention time—days to weeks.

© 2012 Elsevier B.V. All rights reserved.

Contents

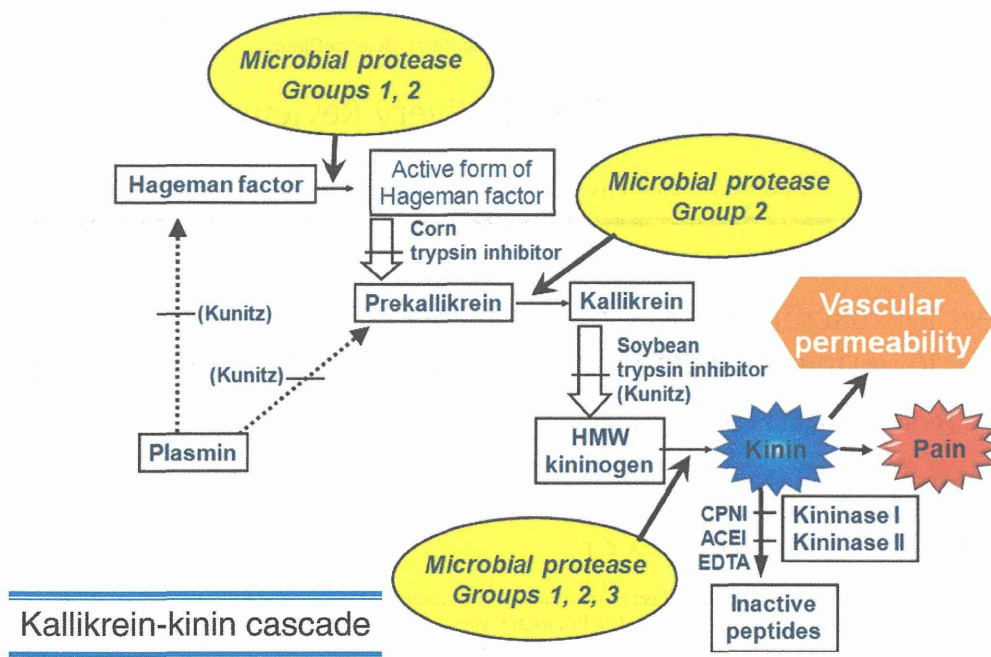## 1. Introduction: vascular permeability in inflammation and cancer

About 30 years ago, we first discovered that vascular permeability in inflammation, that was induced by microbial infections, and triggered by bradykinin (kinin) generation via activation of the proteolytic cascade in the host animals (Fig. 1) [1–5]. We later found that bradykinin was also generated in carcinomatosis and found it was responsible for ascitic and pleural fluid accumulation [6–8]. In addition, we identified many other mediators that were activated simultaneously [9–15], including nitric oxide (NO), prostacyclins, collagenase, and peroxynitrite, which activate matrix metalloproteinase (MMP) (via pro-MMP) and others [11–15].

Fig. 1. The bradykinin-generating protease cascade, which is triggered by bacterial proteases followed by activation of the kallikrein-kinin cascade. The same bradykinin-generating mechanism operates in cancer tissue and in inflamed tissue. A number of protease inhibitors, such as Kunitz-type soybean trypsin inhibitor (Kunitz), corn trypsin inhibitor (Corn), carboxypeptidase N inhibitor (CPNI), angiotensin-converting enzyme inhibitor (ACEI), and ethylenediaminetetraacetic acid (EDTA) inhibit these cascade steps, or consequently potentiate kinin (e.g. ACEI).

We published many reports on the new concept of macromolecular cancer drug delivery, which we named the enhanced permeability and retention (EPR) effect for tumor-selective macromolecular drug targeting [16–23]. Vascular permeability of tumor tissue thus became critically important for the delivery of macromolecular drug based on the EPR effect in cancer treatment.

Fig. 2 presents the various steps involved in drug delivery to tumor tissues and then to tumor cells, and they are the barriers that must be overcome in cancer drug development. The EPR effect, at the first step, is of prime importance because drug extravasation occurs in a tumor-selective manner. Traditional low-molecular-weight (LMW) anticancer drugs have very little tumor selectivity, and most such drugs are widely distributed to normal organs and tissues as well as tumors. Consequently, these anticancer drugs provide insufficient therapeutic benefits and cause severe systemic toxicity, a so-called dose-limited toxicity. By developing tumor-selective anticancer agents, we can avoid this problem.

The present review is intended to overview various aspects of the EPR effect. To demonstrate the EPR effect visually in vivo, tumor selective imaging using fluorophore that is conjugated with macromolecules (fluorescent nanoprobes) and IVIS® imaging system are described later.

Fig. 2. Barriers in the development of cancer selective macromolecular drugs and steps to be overcome.

Advantages of this EPR based macromolecular cancer therapy, without using targeting ligand, is more universal and can be applied to wider tumor spectrum than that using a tumor associated epitope-targeted antibody. In the clinical setting, specific target epitopes of different tumors may be unidentified at early stage of diagnosis. Thus, such therapeutic or diagnostic method may not be as easy as endoscopic visual detection which may be possible with using fluorescent nanoprobes as described later.
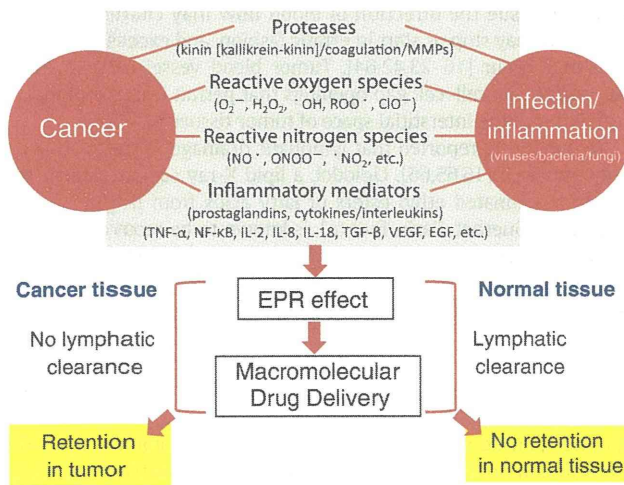
In the past few decades numerous papers were published for tumor targeted delivery of drugs, and imaging using either positron emitting tomography (PET), magnetic resonance imaging (MRI), or fluorescent imaging with fluorophores. Since all these nanoprobes exhibit the EPR effect, such developments are highly advantageous in more efficient treatment and sensitive diagnosis of tumor and inflamed tissues respectively [24–37]. More comprehensive treatise on all these issues may be found in references [31,37].

2. Vascular effectors involved in vascular permeability in cancer and inflammation

Most of these effectors are common mediators in inflammation and cancer (Fig. 3, Table 1) [11–15,17–19] and are highly expressed. Senger et al. [38] and Dvorak et al. [39] found the cancer-specific vascular permeability factor (VPF), which was secreted by tumor cells. VPF was later identified as vascular endothelial growth factor (VEGF) [15,40–42], which in fact enhances the vascular permeability of normal blood vessels as well as that of tumor vessels [15,17], with this process partly involving endothelial nitric oxide synthase (e-NOS) and thus NO.

Bradykinin (kinin) and inhibitors of the kinin-degrading enzyme (kininase), such as angiotensin converting enzyme (ACE) inhibitor [5–8,22], potentiated vascular permeability and the EPR effect. Likewise, generation of oxygen radicals and NO, which is induced during microbial infection and inflammation [10,11,43–45], augmented the EPR effect in cancer. In addition, hypoxic cancer tissues and angina pectoris (or cardiac infarction) demonstrated marked similarity with regard to suppressed vascular blood flow. This observation led to the use of nitroglycerin treatment to improve vascular blood flow and consequently the EPR effect (Fig. 4) [46,47].

These vascular mediators, including activated cyclooxygenase-1, interferon-γ, and inducible NOS (iNOS), as well as other cytokines such as tumor necrosis factor-α (TNF-α), transforming growth factor-β, and interleukin-2 and -8 etc., display cross-talks [15–18,48–53].

Table 1
Factors affecting the EPR effect of macromolecular drugs in solid tumors.[a]

Mediators	Responsible enzymes and mechanisms
Bradykinin	Kallikrein/protease
NO	iNOS
VPF/VEGF	Involved in NO generation
Prostaglandins	Cyclooxygenase 1
Collagenase (MMPs)	Activated from proMMPs by peroxynitrite, or proteases
Peroxynitrite	$NO + O_2^{\cdot -}$
Carbon monoxide (CO)[76]	Heme oxygenase (HO)-1
Induced hypertension	Using angiotensin II
Inflammatory cells and H_2O_2	Neutrophil/NADPH oxidase, etc.
Transforming growth factor (TGF)-β inhibitor[77]	
Tumor necrosis factor (TNF)-α[78]	
Anticancer agents	
Heat[36]	

[a] Extensive production of vascular mediators that facilitate extravasation from normal and tumor vessels, and the enzymes and mechanisms involved in this process (see text for more details).

3. Revisiting the definition of the EPR effect: molecular size, biocompatibility, and surface charge

3.1. Biocompatibility and molecular size

Among the various requirements for and factors influencing the EPR effect, the most important is having a molecular size larger than 40 kDa (Fig. 5, Table 2) [9,16–23,42]. However, this requirement is only partly valid, because size alone is not sufficient for the EPR effect to occur. Biocompatibility may predominate (see Table 2). For instance, most native plasma proteins have a plasma half-life of more than a few days. In contrast, denatured or highly chemically modified plasma proteins are cleared very rapidly. As another example, α_2-macroglobulin (a tetramer of 170 kDa) is an endogenous protease inhibitor in the blood that has a half-life of more than several days. However, the complex of α_2-macroglobulin with plasmin, which is an endogenous serine-type protease that is involved in fibrinolysis, has a half-life of only about 5 min and is cleared very rapidly from the circulation (Table 3) [53,54]. Likewise, certain chemical modifications of albumin result in a much shorter plasma half-life (Table 3).

Fig. 3. Various vascular mediators commonly found in inflammation and cancer that contribute to the EPR effect. These mediators also affect normal blood vessels. A major difference between the two pathological lesions is the clearance rate of extravasated macromolecules such as plasma proteins, lipid particles or nanomedicine, which resulting in a prolonged retention time in tumor tissue compared with that in inflamed tissue.

Fig. 4. (A) Mechanism of NO generation from the nitro agents, nitroglycerin (NG). NO was generated from nitrite, predominantly in hypoxic tumor tissues, not in normal tissues. (B) NG enhanced blood flow seen only in tumor tissue, not in normal tissue. Sarcoma 180 tumor-bearing mice with tumor diameters of 6–7 mm were anesthetized, and the blood flow was measured with a laser flow meter. In this experimental setting, accumulation of the Evans blue-albumin complex increased 2- to 3-fold more than without NG (see text). Adapted from ref. [46].
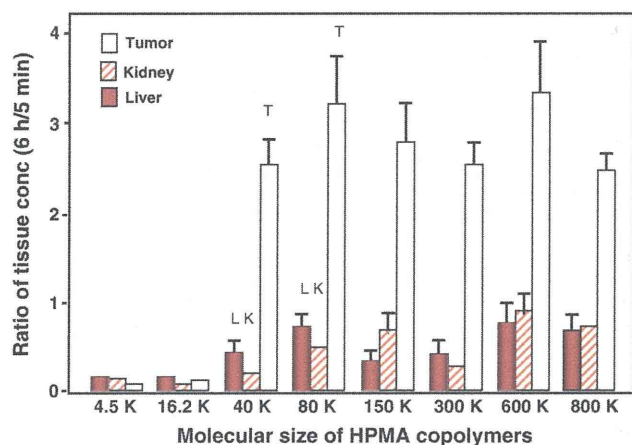
Fig. 5. Tumoritropic uptake of the biocompatible macromolecules, N-(2-hydroxypropyl) methacrylamide (HPMA) polymers containing radioactive ^{131}I-labeled tyrosine were used for this study. The EPR effect leading to higher uptake of the HPMA polymer into tumors is seen for polymer sizes larger than 40 kDa. The amount of uptake at 6 h is compared with that at 5 min. That is, tumor uptake increases with time. Adapted from ref. [20].

This finding suggests the possibility that active ligand-conjugated antibodies will be cleared from the circulation much faster than native proteins or even unmodified biocompatible polymers. This possibility may pose a problem in that an active ligand-targeting strategy and ligand-conjugated product (conjugates) may cause shortened plasma half-lives, the result being not enough time for the EPR effect, which requires a long circulation time.

3.2. Surface charge

The luminal surface of blood vessels is well known to have a negatively charged surface, such as many sulfated and carboxylate sugar moieties [55]. This characteristic means that polymeric drugs with high positive charges will bind nonspecifically to the luminal surface of vascular walls and be rapidly cleared from the blood circulation (Table 4) [56,57]. Particles with high negative charges, however, are known to be trapped in the liver. Also, particles with high negative charges on the solid surface will trigger the coagulation cascade, i.e. Hageman factor is stimulated to become activated Hageman factor (or factor XII → XIIα) (see Fig. 1), which then induces prekallikrein to become kallikrein, followed by conversion of prothrombin to thrombin and activation of the blood coagulation (blood clotting) cascade. Blood coagulation has serious clinical consequences. In the worst case scenario, it may result in disseminated intravascular coagulation, which frequently causes patients to die.

Table 2
Characteristics of the EPR effect of nanomedicines and macromolecular drugs.

Biocompatibility	No interaction with blood components or blood vessels, no antigenicity, no clearance by the reticuloendothelial system, no cell lysis
Molecular size	Larger than 40 kDa (larger than the renal clearance threshold)
Surface charge	Weakly negative to near neutral
Time required to achieve	Longer than several hours in systemic circulation in mice, with distinct accumulation seen at 30 min[16,20]
Drug retention time	Usually days to weeks, in great contrast to passive targeting, in which low-molecular-weight molecules are rapidly cleared and enter the systemic circulation in a few minutes (compare with low-molecular-weight contrast agents)[a]

[a] Compare with low-molecular-weight (LMW) contrast agents in angiography, which is taken up in the tumor tissue by passive targeting, but not retained (see text). Arterial injection of LMW anticancer agents, though they hit tumor by the first path effect, it is not retained in tumor tissue, and so there is not much clinical benefit.

3.3. Hydrophobicity

An important aspect of hydrophobicity is that an increase in hydrophobicity of nanoparticles would result in higher affinity to a cell membrane [58a], and also a much faster endocytotic uptake in parallel with an increase of the cell-association constant to about 10–100 fold [58a,58b]. Further, the environment or pH responsive character of polymeric drugs can be added by utilizing, for instance, maleyl carboxyl group (i.e. hydrophilic-COO⁻ of neutral pH to hydrophobic -COOH at weakly acidic pH) as seen in an SMA-conjugate [58b,58c]. This became more apparent when compared with SMA-micelles vs PEG-conjugated micelles as SMA-micelles were endocytosed about 10 times more than the others [58d].

Hydrophobic polymers with high affinity to cell membranes should also be tested with red blood cells to investigate hemolysis. Also, solubility will be lower as hydrophobicity increases or more side chains are introduced, as we experienced with styrene-co-maleic acid (SMA) copolymer [58a,59]. However, hydrophobicity can be significantly modified by introducing hydrophilic side chain residues, and polymers will become less hemolytic, as we observed with various SMA copolymers.

Another advantage of hydrophobic polymer derivatization is that one can make oily formulation possible. In case of SMANCS, its oily formulation made much higher absorbability after oral administration (×17 times). This indicates one can make pepitedic drugs for oral administration possible by this way [58e].

It should be mentioned that the evaluation of polymeric and nanoparticle drugs for their effect on hemolysis, coagulation, and stability in fresh blood at the early stage of drug development should be carried out for a safely point of view (e.g. ref. [58a]).

4. Defective architecture of tumor blood vessels and lymphatic function

Folkman first documented active angiogenesis in solid tumor many years ago [40,41]. Electron microscopy of a vascular cast of tumor blood vessels that was obtained by using polymer resin showed clear differences between tumor vessels and normal blood vasculature [60–62]. Also, the blood flow volume in tumor tissue is markedly different from that in normal tissue. As noted later in this article (next section), the blood flow volume in normal tissue is consistent, regardless to the blood pressure being modulated by infusion of angiotensin II. However, in tumor tissue, blood flow volume changes (increases) remarkably as angiotensin II is infused to achieve higher blood pressure [63]. Also, in the tumor tissue the direction of blood flow may change abruptly, i.e. the flow may stop or start in erratic fashion, and excessive extravasation may occur [16–23,42,64]. Tumor blood vessels also manifest large endothelial cell–cell gap openings that permit leakage of macromolecules into the interstitial space of tumor tissues [60–62].

We previously reported that lymphatic drainage in tumor tissue is highly impaired [16,65,66]. Lipiodol, a lipid X-ray contrast agent that consists of iodinated ethyl esters of fatty acids from poppy seed oil (Laboratoire Guerbet, Paris, France), is known to be recovered via the lymphatic system in normal tissues. In contrast, however, in tumor tissues, Lipiodol is not recovered easily from the deposited site (cancer tissue), which indicates a lack of or an impaired lymphatic recovery function. Therefore, we took advantage of this tumor-specific retention of Lipiodol for administration of the lipophilic polymer-conjugated anticancer agent SMANCS [neocarzinostatin (NCS) conjugated with the copolymer SMA] in a Lipiodol formulation to treat various tumors, including cancers of liver, kidney, and gallbladder [65–69].

We should note here that water-soluble LMW contrast agents are also taken up preferentially by highly vasculated tumors when infused into the tumor-feeding artery. This technique is used in arterial angiography. Although tumor-selective retention of these LMW contrast agents, or likewise LMW anticancer agents, is observed, that is often called passive tumor-targeting, but it lasts no longer than a

Table 3
Plasma clearance times of selected modified and native proteins in vivo [53,54].[a]

Protein	Species difference, original/test	Probe modification	pI	MW (kDa)	$t_{1/2}$
Albumin	Mouse/mouse	None	4.8	68	72–96 h
Albumin	Mouse/mouse	DTPA (^{51}Cr)	≤4.8	–	6 h
Albumin	Cow/mouse	DTPA (^{51}Cr)	≤4.8	–	1 h
Formaldehyde-modified albumin	Human/rat	^{125}I-labeled formaldehyde	≤4.8	–	25 min
α₂-Macroglobulin	Human/mouse	[125]I	5.3	180×4	140 h
α₂-Macroglobulin-plasmin complex	Human/mouse	[125]I	–	180×4	5 min
Immunoglobulin (IgG)	Mouse/mouse	DTPA	≤6.8	159	60 h
IFN-α	Human/human	None	–	18	8 h (sc)
PEG-IFN-α2a	Human/human	PEG	–	52	80 h (sc)

[a] DTPA, diethylenetriaminepentaacetic acid; IFN, interferon; PEG, polyethylene glycol; sc, given subcutaneously.

few minutes. This characteristic of short time period is in great contrast to that for the EPR effect, in which retention of the lipid particles of Lipiodol or macromolecular drugs persists for a long time, for a few weeks to months [16–18,22,23,42,65–69]. Thus, in contrast to polymeric drugs such as SMANCS/Lipiodol, the LMW contrast agents, or likewise LMW anticancer agents may demonstrate only passive tumor targeting for a very short time, but they will not be retained for substantial periods (*e.g.* days to weeks).

5. Augmentation of the EPR effect and macromolecular drug delivery to tumors

As Table 1 shows, we and others have identified permeability factors, such as bradykinin, NO, and prostaglandins, that facilitate extravasation or the EPR effect in cancer tissues. Generation of these factors does not occur in normal benign tissues, namely, these systems are not activated under normal circumstances. Therefore, augmentation of these factors will affect only tumor or inflamed tissues, with the results being tumor-selective enhanced vascular permeability and improved delivery of drugs to tumors. Nitroglycerin [46,47] and other NO-releasing agents such as isosorbide dinitrate [47] were also effective in enhancing drug delivery in mouse tumor (Fig. 4) (cf. ref. [46]). Nitroglycerin was found also effective when combined with conventional LMW anticancer drugs in clinical setting [70–73].

Augmentation of drug delivery by using an ACE inhibitor such as enalapril was also demonstrated in vivo in mouse tumors (cf. Fig. 1): the ACE inhibitor, when combined with angiotensin II (AT-II)-induced hypertension, enhanced monoclonal antibody (A-7 directed to gastric cancer)-delivery to about 2-fold [42,74]. Dr. Felix Kratz of Freiburg, Germany,

confirmed a similar effect in a different mouse tumor (personal communication).

AT-II-induced hypertension also facilitated drug delivery to other tumor tissues, as shown in animal tumor models [63,75] as well as in patients with advanced or difficult-to-cure cancers (cf. refs. [42,69]). Blood flow dynamics in tumor tissues are quite different from those in normal tissues or organs. That is, no homeostasis of tumor blood flow volume occurs in tumor tissues: when one induced higher blood pressure by infusing AT-II, tumor blood flow volume, as well as tumor drug delivery, increased progressively [63,64,69,75]. Fig. 6 illustrates vascular permeability under AT-II-induced hypertension: in tumors (B), vascular diameters in tumor will dilate, with widened endothelial cell–cell gaps, thus facilitating more drug leakage; whereas in normal blood vessels (A), blood vessels will constrict, endothelial cell–cell junctions will tighten, and less drug leakage will occur, the result being fewer side effects such as bone marrow suppression and gastrointestinal side effects (see Fig. 6) [17,22,63,69,75].
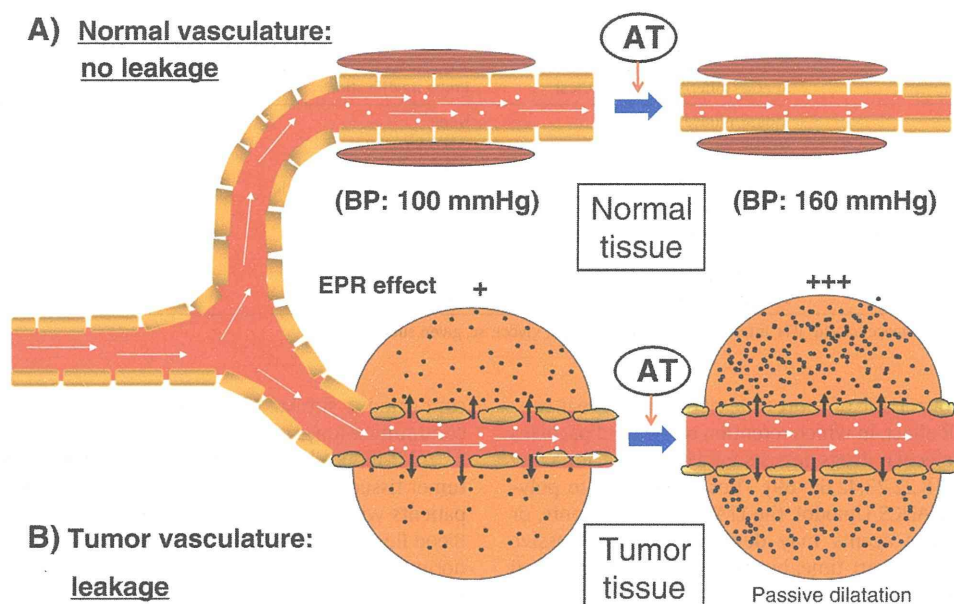
In clinical settings, many cancer drugs are administered at or near the maximum tolerable dose, so a 2- to 3-fold increase in tumor-selective drug delivery would indeed provide great therapeutic benefits [42,68,69,73]. Clinical application of AT-II-induced hypertension during arterial infusion of SMANCS/Lipiodol to patients with difficult-to-cure cancers such as metastatic liver cancer and cancers of the gallbladder, pancreas, and kidney produced very good responses: drug delivery was greatly enhanced, and the time to regression of tumor mass to 50% of the original size became much shortened [69]. In contrast to these favorable results with the arterial infusion of macromolecular drugs such as SMANCS/Lipiodol and AT-II-induced hypertension, the beneficial effect of arterial infusion of conventional LMW drugs is minimal, if not none, due to very rapid diffusion and no drug retention.

Table 4
Surface charge affecting plasma residence times of different nanoparticles in mice [56,57].[a]

Type of nanoparticle	ζ potential (mV)	Mean particle size (nm)	Plasma residence time		Remarks
			$T_{1/2}$	$T_{1/10}$	
Liposome[56]					
Non-PEGylated	−7.31	124	9.08 h	>24 h	Doxorubicin loaded, DPPC:Chol[a] = 1:1
Weakly cationic	+5.58	131	4.51 h	15 h (mean)	Doxorubicin loaded, DPPC:Chol:DC-Chol = 5:4:1, slightly positive
Strongly cationic	+24.25	95	<30 min	<10 min	Doxorubicin loaded, DPPC:DC-Chol = 5:5, strongly positive
PEG-Polylactate nanoparticles[57]					
Weakly anionic	−7.6	90–100	33.8 min	–	PEG chains are on the surface
Strongly anionic	−25.3	90–100	15 min	–	
Strongly anionic	−38.7	90–100	6 min	–	
Chitosan nanoparticle[57]					
Weakly anionic	−13.2	149.2	–	12 h (mean)	CM/MM = 1:2, slightly negative
Strongly anionic	−38.4	156.0	–	3 h (mean)	CM/MM = 2:1, strongly negative
Weakly cationic	+14.8	150.1	–	<1 h	CH/MM = 1:1, slightly positive
Strongly cationic	+34.6	152.7	–	<1 h	CH/MM = 2:1, strongly positive

Data modified from refs. [56] and [57].

[a] DPPC, dipalmitoylphosphatidylcholine; Chol, cholesterol; CM, carboxymethyl chitosan; MM: methyl methacrylate polymer.

A) <u>Normal vasculature:</u> <u>no leakage</u>

(BP: 100 mmHg)   Normal tissue   (BP: 160 mmHg)

EPR effect   +   +++

B) Tumor vasculature: <u>leakage</u>

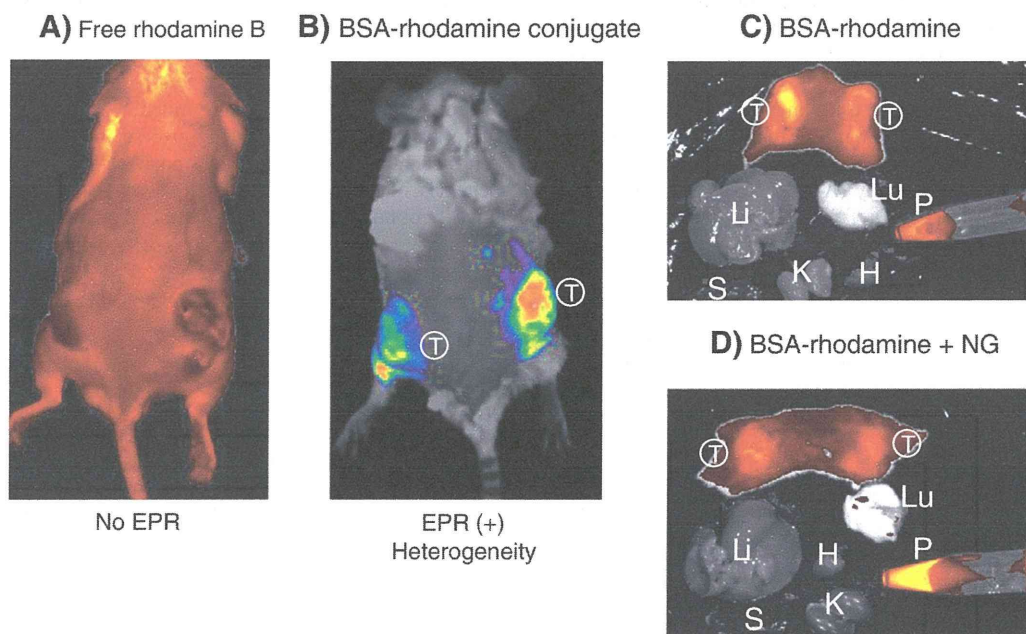Tumor tissue   Passive dilatation

Fig. 6. Diagrammatic representation of the EPR effect and the effect of AT-II-induced hypertension accompanying the enhanced EPR effect and drug delivery in tumor and normal tissue. Under AT-II-induced hypertension (*e.g.* 100 → 160 mmHg), normal vessels and tumor vessels behaved differently. (A) The normal blood vessels have a smooth muscle cell layer that contracts and tightens the cell–cell junctions, and a narrowing of the vascular diameter results in less drug leakage. In tumors (B), the vascular endothelial cell–cell junctions have a wide gap opening that will be opened further by elevating blood pressure hydrodynamically (B, right). AT-II-induced hypertension thus leads to enhanced tumor-selective delivery of macromolecular drugs due to gap opening as demonstrated in clinical settings [68]. Adapted from refs. [18] and [68].

All these above vascular mediators are completely safe for almost all patients, and thus we encourage clinicians to validate this strategy. More recently, heme oxygenase-1 (HO-1)/carbon monoxide (CO) [76], TGF-β inhibitor [77], TNF-α [78] and heat generated by laser (He/Ne) together with gold nanorod [36] are shown to augment the EPR effect in mouse models.

6. Fluorescence imaging and the EPR effect with fluorescent nanoprobes

For our initial observation of the EPR effect (in vivo), we used Evans blue, which we administered by intravenous (i.v.) injection, and the tumor was selectively stained blue [16,19,22,23,42], which we

A) Free rhodamine B   No EPR

B) BSA-rhodamine conjugate   EPR (+) Heterogeneity

C) BSA-rhodamine

D) BSA-rhodamine + NG

Fig. 7. Fluorescence tumor imaging based on EPR effect. The EPR effect-based uptake of fluorescent nanoprobes in tumors is compared with uptake of parental LMW fluorescent probe in vivo. (A) 24 h after i.v. injection of the LMW fluorescent probe, rhodamine B into S-180 tumor-bearing mice, no distinct tumor image is visible. Whereas injection of tetraethyl rhodamine isothiocyanate (TRITC)-conjugated BSA (67 kDa) resulting in highly tumor selective fluorescence at the same experimental conditions. (C) At 24 h, S-180 tumor-bearing mice were dissected, and each organ was viewed with IVIS® system. Only tumor tissues showed significant fluorescence. (D) Same as C except that nitroglycerin (NG) ointment was applied to the skin, and then the EPR effect and tumor drug delivery were evaluated. In D, the cut surface of tumor tissues shows a more homogeneous tumor uptake of fluorescent drug (TRITC-BSA), and also more fluorescent drug remained in the blood, which indicates that the EPR effect would increase progressively with time. In C and D, fluorescence is not seen in all other normal organs. T, tumor; Li, liver; K, kidney; H, heart; S, spleen; Lu, lung; P, plasma.